Acta Cryst. (1998). D**54**, 1377–1381

First Experimental Evidence for Human Dentine Crystal Formation Involving Conversion of Octacalcium Phosphate to Hydroxyapatite

Patricia Bodier-Houllé, Pierre Steuer, Jean-Claude Voegel and Frédéric J. G. Cuisinier*

INSERM U 424, Centre de Recherches Odontologiques, Université Louis Pasteur, 67000 Strasbourg, France. E-mail: fred@odont3.u-strasbg.fr

(*Received 14 July 1997; accepted 20 April 1998*)

Abstract

Biological apatite-crystal formation is a complex process starting with heterogeneous nucleation of inorganic calcium phosphate on an organic extracellular matrix [Cuisinier *et al.* (1995), *J. Cryst. Growth*, **156**, 443–453]. Further stages of crystal growth are also controlled by the organic matrix and both nucleation and growth processes are under cellular control [Mann (1993), *Nature (London)*, **367**, 499–505]. The final mineral in calcified tissue is constituted by poorly crystalline hydroxyapatite (HA) with a low Ca:P ratio, containing foreign ions such as carbonate and fluoride. This study reports the first observation of octacalcium phosphate (OCP) [Brown (1962), *Nature (London)*, **196**, 1048–1055] in a biological tissue; OCP was found in the central part and HA at the extremities of the same crystal of calcifying dentine. This observation is of key importance in understanding the first nucleation steps of biological mineralization. The presence of OCP in a forming human dentine crystal and the observation in the same tissue of nanometer-sized particles with a HA structure [Houllé *et al.* (1997), *J. Dent Res.* **76**, 895–904] clearly proves that two mechanisms, direct nucleation of non-stoichiometric HA crystals and nucleation of OCP, occur simultaneously in same area of mineralization. OCP is found to be a transient phase during the growth of biological crystals. In small crystals, OCP is completely transformed into HA by a hydrolysis reaction (Brown, 1962) and can only be detected in larger crystals because of its slow kinetics of transformation.

1. Introduction

Two distinct mechanisms have been previously proposed for the formation of the biological mineral phase.

(i) Direct nucleation and growth of non-stoichiometric HA crystals (Cuisinier & Voegel, 1994; Cuisinier *et al.*, 1993, 1994, 1995; Houllé *et al.*, 1997).

(ii) Nucleation of different calcium phosphate phases, mainly octacalcium phosphate (OCP) (Brown, 1962; Nelson & Barry, 1989) or amorphous calcium phosphate (ACP) (Glimcher, 1984). Such phases can be transformed into HA by a chemical reaction.

The first mechanism, involving direct formation of HA crystals, is supported by recent high-resolution electron microscopy (HREM) studies of different calcified tissues. Nanometer-sized particles were observed in human enamel (Cuisinier, Voegel *et al.*, 1992; Cuisinier, Steuer *et al.*, 1992; Cuisinier *et al.*, 1993), dentine (Houllé *et al.*, 1997) and chicken bone (Cuisinier *et al.*, 1995). A four-step mechanism was proposed to describe the conversion of the nanometer-sized HA crystals to final adult HA crystals (Cuisinier *et al.*, 1995). The two initial stages consist of ionic adsorption and nucleation of nanometer-sized particles on specific nucleation sites. Each site is confined to a discrete area at the matrix surface. These sites could be distinct structural electrostatic and topographical domains that tailor interfacial interaction between the matrix and the mineral nuclei. The effect is to minimize nucleation energy and to control the structure and orientation of nanoparticles. The mechanism by which calcium phosphate ions accumulate in localized areas and in an ordered pattern is unknown. The size and morphology of the nanoparticles are strongly dependent on the interplay between the ligand surface of the protein and the crystal lattice energies (Meldrum *et al.*, 1991). A great similarity seems to exist between the nanometer-sized particles observed in the first crystallization stages of ceramics (Ramos & Gandais, 1989), the metallic nanoparticles deposited on amorphous films (Artal *et al.*, 1992) and the biological nanoparticles found in enamel and bone. The structural identity between the nanoparticle and the final crystal is a strong argument supporting HA nanoparticles constituting a genuine step in the biological formation of HA crystals. In the third step of biological crystal development the stable nanometer-sized HA particles appear to grow by further ionic deposition. The growth direction seems to be governed by the matrix and the neighbouring particles growing on the same matrix. These particles consequently fuse together owing to space restriction. The last stage observed for bone-crystal growth is a lateral fusion of ribbon-like crystals by their (100) faces mediated by high-angle grain boundaries. Such boundaries, resulting from the fusion of crystals disoriented by more than 5°, present complex atomic structures. The final develop-

ment stage could then simply result from constraints imposed by the organic framework which limit the space available for lateral growth.

The second mechanism for biological crystals was proposed by Brown (1962, 1965) and involves the growth of biological apatites depending on the presence of OCP, which has a transitory existence. This mechanism suggests that the first step is the formation of a two-dimensional nucleus of OCP, one unit-cell thick, which subsequently grows to HA (Brown, 1965; Nelson & McLean, 1984). The thin plate-like morphology of OCP crystals is consistent with the ribbon-like structure of the initial enamel crystal (Cuisinier, Voegel *et al.*, 1992; Cuisinier, Steuer *et al.*, 1992; Weiss *et al.*, 1981) and with the plate-like structures of bone (Cuisinier *et al.*, 1987) and dentine crystals (Schroeder & Frank, 1985). The fact that OCP hydrolysis forms carbonated HA strengthens this hypothesis. Until now, the only experimental indication for the existence of OCP in calcifying bones and teeth was given by Raman spectroscopy of extracellular matrix vesicles (Sauer *et al.*, 1994) where the first distinct mineral observed had phosphate bonds similar to those found in OCP but clearly different from ACP and HA. Other indirect methods based on Ca:P ratio measurements (Kodaka & Miake, 1991; Kodaka *et al.*, 1992; Paschalis *et al.*, 1996) or morphology analyses (LeGeros *et al.*, 1988; Miake *et al.*, 1995) and equidistance measurements (Weiss *et al.*, 1981; Tohda *et al.*, 1997) were used to explore the possible presence of OCP in calcified tissues.

The aim of this study is to observe the presence of OCP as a precursor phase for HA during human dentine crystal formation.

2. Materials and methods

Incisors and molars were collected from five-month-old human aborted foetuses (Gynaecological Department, Université Louis Pasteur, Strasbourg, France) according a protocol conforming to university standards. They were fixed for 3 h in a 2% glutaraldehyde and 2% paraformaldehyde solution in 0.1 *M* sodium cacodylate buffer at pH 7.4. After 2 h of post-fixation in 1% OsO_4 solution in the same buffer, the specimens were embedded in Epon 812.

Non-decalcified ultrathin sections were obtained with a MT-2b Sorvall–Porter microtome equipped with a diamond knife. The sections were floated on water at a pH value close to neutrality and saturated against synthetic HA (200 mg l^{-1}) (Biogel HTP hydroxyapatites, Biorad Laboratory, Hercules, CA, USA) in order to prevent spurious crystal dissolution.

2.1. *HREM*

The sections were observed in an EM 430 ST transmission electron microscope (Philips, Eindhoven, The Netherlands) operating at 300 kV, using a double-tilt specimen holder and a nitrogen-cooled anti-contamination device without further staining. The microscope possesses a spherical aberration constant of 1.1 mm and a Scherzer resolution of 0.19 nm. The micrographs were recorded on SO163 films (KODAK, Rochester, USA). For each individual characteristic image, the absence of astigmatism and drift was checked on a laser bench (Micro-contrôle, Evry, France).

2.2. *HREM image simulation*

HREM images were simulated with a Silicon Graphics (Mountain View, CA, USA) workstation using the *EMS* program (Stadelmann, 1987). Simulated images were calculated by the multislice method using the atomic positions of HA (Kay *et al.*, 1964).

2.3. *HREM image digitalization*

In order to proceed to numerical analyses, selected micrographs were digitalized at the SERTIT (Service Regional de Traitement d'Image et de Télédétection, Strasbourg, France). A high-resolution drum microdensitometer (WIRTH 105D, Frankfurt am Main, Germany) was used to perform the image-density measurements (256 grey levels) with steps of 25 μm.

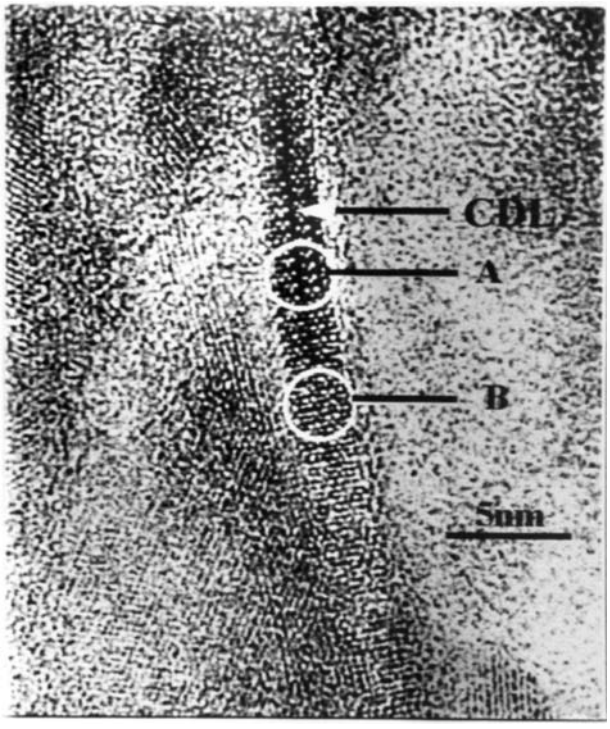

Fig. 1. Human dentine crystal situated at the mineralization front. The dentine crystal has a needle-like structure and its long axis is crossed by a central dark line (CDL). Two white circles (A and B) correspond to the analysis of the two sites where two-dimensional fast Fourier transforms were performed.

Numerical diffractograms were realised by two-dimensional fast Fourier transform operations with the *Khoros* image-analysis package (Khoral Research Inc., Albuquerque, USA; http://www.khoral.com).

3. Results

Human dentine samples were explored in areas where nascent crystals appear. These areas correspond to the mineralization front and a dentine crystal presenting a ribbon-like structure was found (Fig. 1). This crystal has a thickness of 1.6 nm and in its central part a dark line parallel to the crystal axis was noted. This line has a very similar aspect to the well known central dark line (CDL) observed in different biological crystals (Weiss *et al.*, 1981, Cuisinier *et al.*, 1987) and ends before reaching the crystal extremities.

The two numerical diffractograms *A* and *B* presented in Fig. 2 were realised by two-dimensional fast Fourier transform. Diffractogram *A* corresponds to the central part of the dentine crystal and diffractogram *B* to the area located at the lower extremity of the crystal. The comparison between both numerical and calculated diffractograms allowed the identification of the following zone axes: (101) of OCP for area *A* (Brown, 1962) and (101) of HA for area *B* (Kay *et al.*, 1964). To determine the structure of this crystal in both areas we performed a series of HREM image simulations using the structural data of HA and OCP. The good correspondence between the calculated image of HA and the crystal lattice of the extremity of the crystal shows that the crystal possesses, at both extremities, a structure related to HA (Fig. 3). In the central part, the crystal has a structure related to OCP, as proven by the good correspondence between the calculated and experimental images.

4. Discussion

The present observations constitute the first direct evidence of the presence of OCP in calcifying bones or teeth since Brown (1962) stated that OCP should be a precursor phase of HA during biological crystal formation. Previously, the study by Nelson *et al.* (1986) was the only direct structural proof of the presence of OCP, but this was observed in synthetic calcium phosphate crystals. OCP has been proposed to be the precursor of HA based on Ca:P ratio measurements (Kodaka & Miake, 1991; Kodaka *et al.*, 1992; Paschalis *et al.*, 1996). Also, Tomson *et al.* (1977) have found that the new mineral formed in dentine has a stoichiometry close to OCP. Other studies using Ca:P ratio measurements completed by morphology analyses (LeGeros *et al.*, 1988; Miake *et al.*, 1995), equidistance measurements (Weiss *et al.*, 1981; Tohda *et al.*, 1997), defect exploration in synthetic tissue (Nelson *et al.*, 1986) or in biological tissue (Cuisinier *et al.*, 1992) also came to the conclusion that OCP should be present in specific situations as a transitory precursor of HA. In the last 35 years OCP has more often been found in pathological situations such as in dental calculi (Kodaka & Miake, 1991; Kodaka *et al.*, 1992) or in experimental stimulation of osteogenesis (Suzuki *et al.*, 1991; Sasano *et al.*, 1995), as the formation and stabilization of OCP is facilitated by a low pH value and a temperature increase (LeGeros *et al.*, 1984; Johnsson & Nancollas, 1992).

However, we must underline that this study constitutes the first evidence for the presence, in the same biological crystal, of two different calcium phosphate

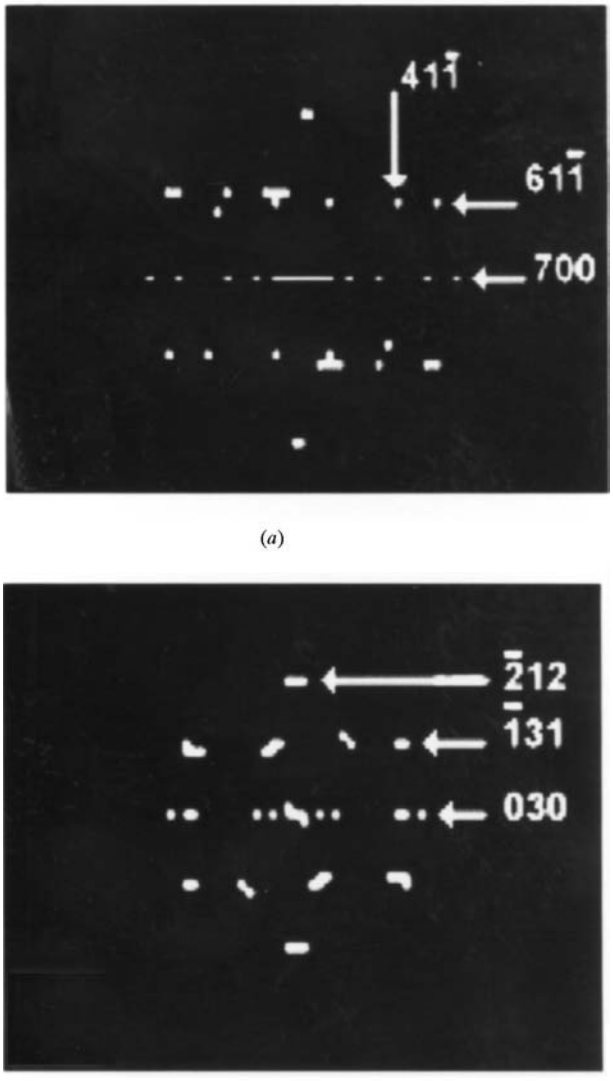

Fig. 2. Numerical diffractograms of two areas from Fig. 1. Diffractogram *A* (*a*) corresponds to the central part of the dentine crystal of Fig. 1 and diffractogram *B* (*b*) to the area situated at the lower extremity of the crystal. The comparison between numerical and calculated diffractograms allows the identification of the zone axis: (101) of OCP for area *A* and (101) of HA for area *B*.

phases: OCP in its central part and HA at its extremities. In the observed crystal, OCP inclusion appears as the well known central dark line (CDL) (Frazier, 1968; Rönnholm, 1962). CDLs were previously described in mature enamel crystals (Rönnholm, 1962; Marshall & Lawless, 1981) and in growth rate enamel crystals (Nakahara & Kakei, 1983) as well as in other calcified tissues (Nakahara & Kakei, 1984) and were generally described as 'planar structures', but no direct evidence about the molecular structure of the line was given. Previously, two hypotheses have been advanced to elucidate their origin. (i) CDLs could be created by local crystallographic variations. A theoretical approach showed that CDLs could be attributed to bi-directional defects such as boundaries (Brès *et al.*, 1986), which have been observed in mature enamel crystals (Brès *et al.*, 1990) but could not absolutely be correlated to CDLs. (ii) CDLs were also attributed to ionic substitutions, such as carbonate incorporations, in the centre of the crystals (Brès *et al.*, 1990). CDLs are always localized in crystal centres and, therefore, appear to be linked to the initial crystal-growth mechanisms. Our observations also show, for the first time, that the CDL corresponds closely with the so-called water layer of OCP (Brown, 1962; Tomazic *et al.*, 1989).

The great sensitivity of OCP to temperature increase, induced either by electron beam or by inclusion, which favours hydrolysis into defective HA, was often advanced to explain the absence of OCP in previous HREM observations of *in vivo* tissues (Cuisinier, Voegel *et al.*, 1992; Cuisinier, Steuer *et al.*, 1992). This indicates that the present observations could neither be induced by electron-beam irradiation nor be an artifact. This was also strongly supported by *in vitro* studies where OCP was detected between HA layers using HREM techniques (Nelson & McLean, 1984; Ijima, Tohda & Moriwaki, 1992; Ijima, Tohda, Suzuki *et al.*, 1992).

The hydrolysis of OCP into HA was proposed to occur during biological crystal formation (Brown, 1965; Tung & Brown, 1985). For *in vitro* systems it was found that hydrolysis was never complete except for very small OCP crystals (Nelson & McLean, 1984; Tung & Brown, 1985). The chemical reaction, consisting of calcium diffusion into the hydrolyzing crystal and the removal of water molecules, could be incomplete owing to the slow kinetics (LeGeros *et al.*, 1989). Our observations suggest that the hydrolysis of OCP in the formation of biological crystals develops along (100) crystal planes and not in a perpendicular direction.

From the observation of the growth of this dentine crystal a three-step mechanism was proposed:

(i) initial formation of an unit-cell-thick OCP crystal;

(ii) hydrolysis of OCP along the (100) planes;

(iii) deposition of HA on the (100) OCP planes (Fig. 4).

Depending on the relative kinetic rates of the two last steps, the process can either lead to the formation of HA without any detectable OCP inclusion [step (ii) faster than step (iii)] or to the formation of HA crystals with

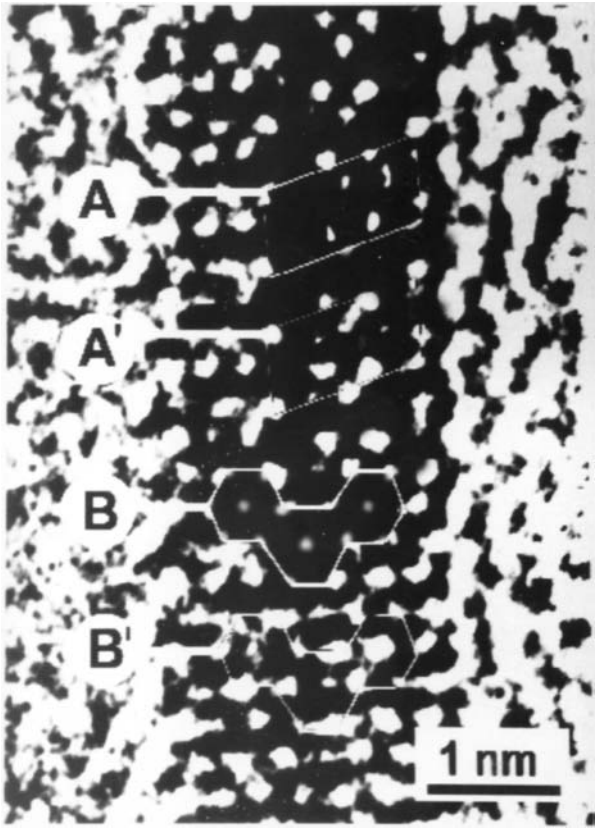

Fig. 3. Higher magnification of the crystal shown in Fig. 1. Insert *A* is a calculated image with OCP structural parameters and insert *B* a calculated image with HA structural parameters. *A'* and *B'* correspond to areas identical to *A* and *B* in direct space. *A* and *B* images were calculated using the *EMS* program (Stadelmann, 1987) on a Silicon Graphics Indigo 2 station using the multislice method. The structural data for image calculations are thickness 6 nm and defocalization 105 nm^{-1} for *A*, and thickness 1.4 nm and defocalization 98 nm^{-1} for *B*.

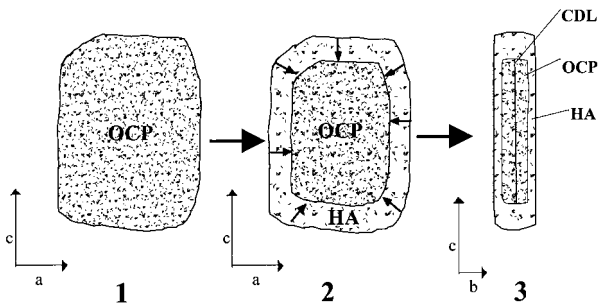

Fig. 4. Three-step mechanism of biological crystal formation with OCP as an intermediate calcium phosphate phase. (1) Formation of a one unit-cell-thick OCP crystal. (2) OCP hydrolysis into HA along the (100) plane; arrows, direction of hydrolysis. (3) HA formation on the (100) face of the OCP–HA crystal.

OCP incorporated in the crystal centre [step (ii) slower than step (iii)].

On the basis of thermodynamic analysis, Nelson & MacLean (1984) showed that initially the nucleation of OCP or HA was equiprobable. The observation of both OCP and HA particles in the same spatial and temporal loci is understandable. The existence of nanoparticles with an HA structure (Cuisinier *et al.*, 1995; Houllé *et al.*, 1997) is induced either by a direct HA precipitation or by the rapid conversion of OCP into HA. OCP should be detectable in other biological calcified tissue because the first step (heterogeneous nucleation) of their mineralization processes are identical.

Similar identifications of OCP within other biological crystals and the determination of the driving force for OCP conversion in such systems could constitute one of the next targets in obtaining a better knowledge of the mineralization process in biological apatites.

We thank M. Romeo for is help in image analysis and E. Mann for reviewing the manuscript.

References

Artal, P., Avolos-Borja, M., Soria, F., Poppa, H. & Heinemann, K. (1992). *Ultramicroscopy*, **30**, 405–416.

Brès, E. F., Hutchinson, J. L., Voegel, J. C. & Frank, R. M. (1990). *Colloq. Phys. Cl. (Suppl. 1)* **51**, 97–102.

Brès, E. F., Waddington, W. G., Voegel, J. C., Barry J. C. & Frank R. M. (1986). *Biophys. J.* 1105–1193.

Brown, W. E. (1962). *Nature (London)*, **196**, 1048–1055.

Brown, W. E. (1965). *Tooth Enamel I*, edited by M. V. Stack & R. W. Fearnhead, pp. 11–14. Bristol: John Wright.

Cuisinier, F. J. G., Brès, E. F., Hemmerlé, J., Voegel, J. C. & Frank, R. M. (1987). *Calcif. Tissue Int.* **40**, 332–338.

Cuisinier, F. J. G., Steuer, P., Brisson, A. & Voegel, J. C. (1995). *J. Cryst. Growth*, **156**, 443–453.

Cuisinier, F. J. G., Steuer, P., Senger, B., Voegel, J. C. & Frank, R. M. (1992). *Calcif. Tissue Int.* **51**, 259–268.

Cuisinier, F. J. G., Steuer, P., Senger, B., Voegel, J. C. & Frank, R. M. (1993). *Cell. Tissue Res.* **273**, 175–182.

Cuisinier, F. J. G. & Voegel, J. C. (1994). *Curr. Topics Crystal Growth Res.* **1**, 229–243.

Cuisinier, F. J. G., Voegel, J. C., Yacaman, J. & Frank, R. M. (1992). *J. Cryst. Growth*, **116**, 314–318.

Frazier, P. D. (1968). *J. Ultrastruct. Res.* **22**, 1–11.

Glimcher, M. J. (1984). *Philos. Trans. R. Soc. London Ser. B*, **304**, 479–508.

Houllé, P., Voegel, J. C., Schultz, P. & Cuisinier, F. J. G. (1997). *J. Dent. Res.* **76**, 895–904.

Iijima, M., Tohda, H. & Moriwaki, Y. (1992). *J. Cryst. Growth*, **116**, 319–326.

Iijima, M., Tohda, H., Suzuki, Y., Yanagisawa, T. & Moriwaki, Y. (1992). *Calcif. Tissue Int.* **50**, 357–361.

Johnsson, M. S. & Nancollas, G. H. (1992). *Crit. Rev. Oral Biol. Med.* **3**, 61–82.

Kay, M. I., Young, R. A. & Posner, A. S. (1964). *Nature (London)*, **204**, 1050–1052.

Kodaka, T. & Miake, Y. (1991). *Bull. Tokyo Dent. Collect.* **32**(3), 99–110.

Kodaka, T., Ohohara, Y. & Debari, K. (1992). *Scanning Microsc.* **6**, 475–486.

LeGeros, R. Z., Daculsi, G., Orly, I., Abergas, T. & Torres, W. (1989). *Scanning Microsc.* **3**, 129–138.

LeGeros, R. Z., Ijkowska, R. & LeGeros, J. P. (1984). *Scanning Electron Microsc.* **4**, 1771–1777.

LeGeros, R. Z., Orly, I., LeGeros, J. P., Gomez, C., Kazimiroff, J., Tarpley, T. & Kerebel, B. (1988). *Scanning Microsc.* **2**, 346–356.

Mann, S. (1993). *Nature (London)*, **367**, 499–505.

Marshall, A. F. & Lawless, K. R. (1981). *J. Dent. Res.* **60**, 1773–1782.

Meldrum, F. C., Wade, U. J., Nimmo, D. L., Heywood, B. R. & Mann, S. (1991). *Nature (London)*, **349**, 684–687.

Miake, Y., Yanagisawa, T., Yajima, Y., Noma, H. & Nonami T. (1995). *J. Dent. Res.* **74**, 1756–1763.

Nakahara, H. & Kakei, M. (1983). *Bull. Josai Dent. University*, **12**, 1–7.

Nakahara, H. & Kakei, M. (1984). *Josai Shika Daigaku Kiyo*, **13**, 259–263.

Nelson, D. G. A. & Barry, J. C. (1989). *Anat. Rec.* **224**, 265–276.

Nelson, D. G. A. & McLean, J. D. (1984). *Calcif. Tissue Int.* **36**, 219–232.

Nelson, D. G. A., Wood, G. J., Barry, J. C. & Featherstone, J. D. (1986). *Ultramicroscopy*, **19**, 253–266.

Paschalis, E. P., Tan, J. & Nancollas, G. H. (1996). *J. Dent. Res.* **75**, 1019–1026.

Ramos, A. & Gandais, M. (1989). *J. Electron Microsc. Tech.* **11**, 238–241.

Rönnholm, E. (1962). *J. Ultrastruct. Res.* **6**, 249–303.

Sasano, Y., Kamakura, S., Nakamura, M., Suzuki, O., Mizoguchi, I., Akita, H. & Kagayama, M. (1995). *Anat. Rec.* **242**, 40–46.

Sauer, G. R., Zunic, W. B., Durig, J. R. & Wuthier, R. E. (1994). *Calcif. Tissue. Int.* **54**, 414–420.

Schroeder, L. & Frank, R. M. (1985). *Cell. Tissue Res.* **242**, 449–451.

Stadelmann, P. (1987). *Ultramicroscopy*, **21**, 131–146.

Suzuki, O., Nakamura, M., Miyasaka, Y., Kagayama, M. & Sakurai, M. (1991). *Tokohu J. Exp. Med.* **164**, 37–50.

Tohda, H., Yamada, M., Yamaguchi, Y. & Yanagisawa, T. (1997). *J. Electron Microsc.* **1**, 97–101.

Tomazic, B. B., Tung, M. S., Gregory, T. M. & Brown, W. E. (1989). *Scanning Microsc.* **3**, 119–127.

Tomson, M. B., Tomazic, B. B., Nancollas, G. H., Miller, W. & Everett, M. (1977). *J. Dent. Res.* **56**, 1369–1375.

Tung, M. S. & Brown, W. E. (1985). *Calcif. Tissue Int.* **37**, 329–331.

Weiss, M. P., Voegel, J. C. & Frank, R. M. (1981). *J. Ultrastruct. Res.* **76**, 286–292.